Program Digest, 2019 IEEE International Ultrasonics Symposium (IUS)
Glasgow, Scotland, October 6-9, 2019

Axial Super-Resolution in Ultrasound Imaging

Saurav Kumaraswami Shastri
Department of Electrical Engineering
Indian Institute of Science
Bengaluru, India
sauravs@iisc.ac.in

Sunil Rudresh
Department of Electrical Engineering
Indian Institute of Science
Bengaluru, India
sunilr@iisc.ac.in

Ramkumar Anand
Department of Applied Mechanics
Indian Institute of Technology Madras
Chennai, India
am15d026@smail.iitm.ac.in

Sudarshan Nagesh
Zendar Co.,
Berkeley, USA
sudarshannagesh90@gmail.com

Dibbyan Mazumder
Martinos Center for Biomedical Imaging
Harvard Medical School and
Massachusetts General Hospital
Charlestown, USA
dibbyan@gmail.com

Arun K. Thittai
Department of Applied Mechanics
Indian Institute of Technology Madras
Chennai, India
akthittai@iitm.ac.in

Chandra Sekhar Seelamantula
Department of Electrical Engineering
Indian Institute of Science
Bengaluru, India
css@iisc.ac.in

***Abstract*—A fundamental challenge in non-destructive evaluation using ultrasound is to accurately estimate the thicknesses of different layers or cracks present in the object being probed. This inherently corresponds to localizing the point-sources of the reflections from the received signal. Conventional signal processing techniques cannot resolve reflectors whose spacing is below the axial resolution limit, which is of the order of the wavelength of the probing pulse. The objective of this paper is to demonstrate axial super-resolution capability using both simulated and experimental ultrasound data. We show that the ultrasound reflections could be modelled effectively as FRI signals, which can be sampled at sub-Nyquist rates. The FRI sampling method brings the reconstruction problem within a parametric estimation framework, for which efficient high-resolution spectral estimation techniques are available. We experimentally demonstrate that the proposed technique is able to resolve the thicknesses of layers of custom designed Agarose phantoms that are up to 2.25 times below the conventional resolution limit.**

***Index Terms*—Non-destructive evaluation, ultrasound imaging, axial resolution, super-resolution, finite-rate-of-innovation, sub-Nyquist sampling.**

I. Introduction

As a non-invasive imaging modality, ultrasound has been popularly used for medical imaging and non-destructive evaluation (NDE) of objects. In ultrasound imaging for NDE, objects are probed by high frequency sound waves to analyze their structural details. The reflected signals (echoes) collected at the receiver correspond to the boundaries of the layers having different acoustic impedances. The time-of-flight (ToF) principle is then applied on the received ultrasound signals to obtain the acoustic image of the object being probed. In this paper, we mainly concentrate on the 1-D ultrasound imaging for NDE applications such as finding the location of cracks in a material or measuring the thickness of an object or the various layers in a composite object.

This work has been funded by the Ministry of Human Resource Development - IMPacting Research INnovation and Technology (IMPRINT), Government of India (project number IMPR-6000).

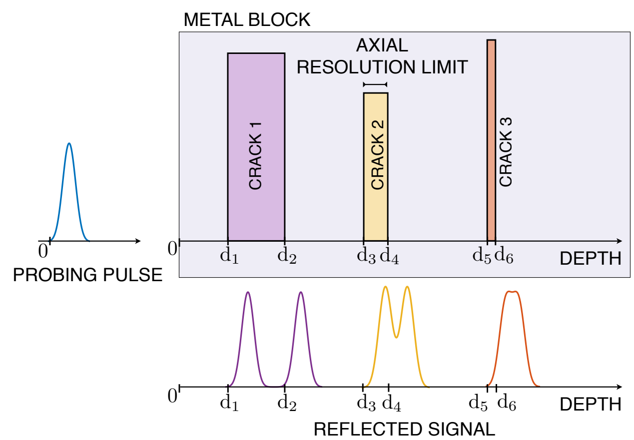

Fig. 1: [Color online] An illustration of ultrasound based non-destructive evaluation of a specimen having cracks of different thicknesses. Only envelopes of the signals are shown to aid readability.

The axial resolution limit is defined as the smallest distance between two point reflectors in the direction of propagation of the ultrasound signals that can be reliably estimated. As in illustration, consider the setup shown in Fig. 1. The metal block has three cracks of different widths. A probing ultrasound pulse is transmitted axially into the metal block. The reflected signal consists of six peaks one corresponding to each *acoustic interface*. Based on the widths of the cracks, the reflected pulses may be well-resolved (violet), at the limit of resolution (yellow), or unresolved (orange). The axial resolution limit (D) for an ultrasound system depends on the *spatial pulse length* (SPL) of the transmitted pulse and is given as [1]

$$D = \frac{\mathrm{SPL}}{2}. \tag{1}$$

Consequently, smaller the SPL, better the resolution. However, a pulse having a smaller SPL has higher bandwidth, and this requires higher sampling rate, which leads to increased data processing needs. A standard ultrasound reconstruction technique is not capable of *super-resolving* overlapping pulses i.e., it cannot localize the reflectors spaced below the axial resolution limit D, and hence is not suitable for determining thicknesses of thin layers. In this paper, we address the problem of improving the axial resolution in 1-D ultrasound imaging by modelling the reflected ultrasound signal as a *finite-rate-of-innovation* (FRI) signal [2]. We also demonstrate the *super-resolution* capability of the proposed technique on simulated and experimental ultrasound data. The FRI model also paves the way to sample and reconstruct ultrasound signals at sub-Nyquist rates.

A. Prior work

Salazar et al. [3] and Oelze [4] employed pulse cancellation and pulse compression techniques, respectively, to decrease the SPL of the ultrasound pulse in order to improve the axial resolution. However, decreasing the SPL limits the penetration depth and the signal-to-noise ratio (SNR) of the reflected signal. To overcome this limitation, the 1-D reflected ultrasound signals have been extensively modelled as a convolution between the transmitted pulse and the acoustic reflectivity function [5], [6], and to loacalize the reflectors, various deconvolution-based techniques [7] have been proposed in the literature. With the knowledge of the transmitted pulse shape, the deconvolution can be solved using ℓ_1-norm minimization approach [5] since the reflectivity function is generally sparse. However, the ultrasound signals have to be sampled at a very high rate to ensure finely discretized grid in order to accurately estimate the location of the reflectors.

Recently, Tur et al. [8] invoked the *finite-rate-of-innovation (FRI)* model for the ultrasound signal and performed reconstruction at sub-Nyquist rates. Wagner et al. [9] and Chernyakova et al. [10] proposed beamforming of the sub-Nyquist measurements in the time and frequency domains, respectively. In our previous work [11], we demonstrated FRI-based 2-D medical ultrasound image reconstruction using a sophisticated sampling kernel. Next, we briefly present the FRI sampling and reconstruction framework, which is central to this paper.

II. FRI SAMPLING AND RECONSTRUCTION

The FRI sampling and reconstruction problem can be formally stated as follows: Given uniform measurements of the signal

$$x(t) = \sum_{\ell=1}^{L} a_\ell \, h(t - t_\ell), \tag{2}$$

observed through a sampling kernel $g(t)$ (cf. Fig. 2), estimate $\{a_\ell, t_\ell\}_{\ell=1}^{L}$ assuming that $h(t)$ is known. Without loss of generality, assume that $t_1 < t_2 < t_3 < \cdots t_{L-1} < t_L$. In the illustration shown in Fig. 1, the reflected signal can be modelled as a sum of delayed versions of the probing pulse with $L = 6$, where each delay corresponds to the location of an acoustic interface. The continuous-time Fourier

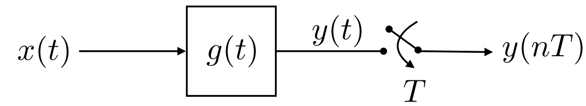

Fig. 2: A schematic of kernel-based sampling framework.

transform (CTFT) of $x(t)$ in (2) is $\hat{x}(\omega) = \hat{h}(\omega) \sum_{\ell=1}^{L} a_\ell \, e^{-\mathrm{j}\omega t_\ell}$.

Consider the frequency-domain sequence

$$\hat{r}(k\omega_0) \;=\; \frac{\hat{x}(k\omega_0)}{\hat{h}(k\omega_0)} = \sum_{\ell=1}^{L} a_\ell \, e^{-\mathrm{j}k\omega_0 t_\ell}, \tag{3}$$

where $k \in \mathbb{Z}$ and $\omega_0 \in \mathbb{R}^+$ are chosen such that $\hat{h}(k\omega_0) \neq 0$. Now, given $\hat{r}(k\omega_0)$ for a set of contiguous values of k with the condition that $|\omega_0 t_L| < 2\pi$, one can apply high-resolution spectral estimation (HRSE) techniques [12] to estimate $\{a_\ell, t_\ell\}_{\ell=1}^{L}$.

A. Sampling Kernel

In (3), $\hat{h}(k\omega_0)$ can be computed a priori as $h(t)$ is known, and hence one needs the CTFT values of $x(t)$ at frequencies $\{k\omega_0, \; k \in \mathcal{K}\}$. The sampling kernel $g(t)$ (cf. Fig.2) is designed such that it avoids aliasing at these frequencies thus allowing for the computation of $\hat{x}(k\omega_0)$. The filtered signal $y(t)$ is sampled with a sampling period T such that the discrete-time Fourier transform (DTFT) of the samples $\{y(nT)\}$ matches the CTFT values of $x(t)$ at the frequencies $\{k\omega_0, \, k \in \mathcal{K}\}$.

Of the several sampling kernels proposed over the past two decades, the one that is of particular interest to us is the non-repeating SoS kernel that can be used for sampling of both periodic and non-periodic FRI signals [11]. The impulse response and the frequency response of the compactly supported non-repeating SoS (NR-SoS) kernel are given by

$$g(t) \;=\; \frac{1}{T_0}\mathrm{rect}\left(\frac{t}{T_0}\right) \sum_{k=-K}^{K} e^{\mathrm{j}k\omega_0 t}, \quad \text{and} \tag{4}$$

$$\hat{g}(\omega) \;=\; \sum_{k=-K}^{K} \mathrm{sinc}\left(\frac{\omega}{\omega_0} - k\right), \tag{5}$$

respectively, where $\mathrm{rect}\left(\frac{t}{T_0}\right) = 1$ for $t \in \left[-\frac{T_0}{2}, \frac{T_0}{2}\right]$ and zero elsewhere, and $\omega_0 = \frac{2\pi}{T_0}$. It can be shown that by sampling the filtered signal $y(t)$ at the rate $\omega_s \geq (2L+1)\omega_0$, one can estimate the parameters of the input signal $x(t)$ accurately in the absence of noise [11]. In the presence of noise, prior to the application of the HRSE algorithms, Cadzow's denoising algorithm [13] is applied on the noisy $\{\hat{r}(k\omega_0)\}$ to suppress the effect of noise and modelling errors.

III. SIMULATION RESULTS

To demonstrate the application of the FRI sampling framework for NDE applications, we simulated an ultrasound setup using the Field-II [14], [15] software. We considered a Gaussian-modulated sinusoidal pulse as the transmitted pulse. The center frequency and the -6 dB bandwidth of the pulse

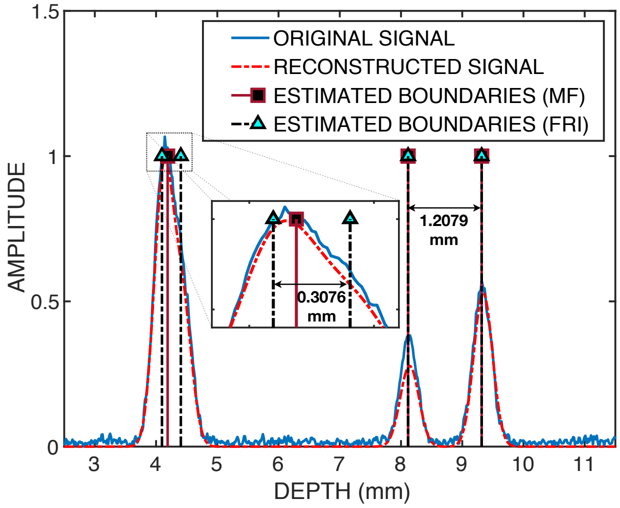

Fig. 3: [Color online] Envelopes of the original and FRI reconstructed ultrasound signals along with the estimated locations of the point reflectors. The FRI technique is able to resolve the pair of pins separated by 0.3 mm, whereas MF technique is not.

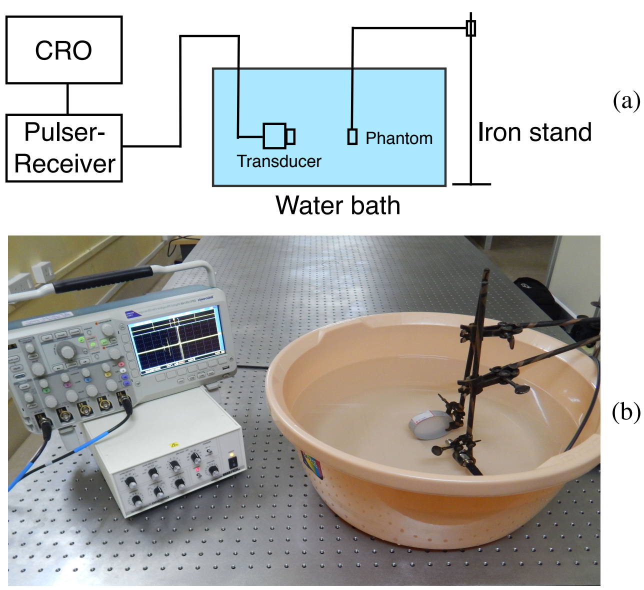

Fig. 4: [Color online] (a) A schematic showing the experimental setup used to image Agarose phantoms; and (b) a picture of the experimental setup.

were set to 5.05 MHz and 2 MHz, respectively. The SPL of the transmitted pulse was computed to be 1.14 mm, and by using (1) the resolution limit of the system was computed to be $D = 0.57$ mm. For the simulation, we considered a resolution phantom consisting of two pairs of pins. The pins in the first and the second pairs were separated by 0.3 mm and 1.2 mm, respectively to simulate unresolved and well-resolved cases. The SNR of the reflected signal was kept at 20 dB.

For sampling, we employed the non-repeating SoS sampling kernel and computed $|\mathcal{K}| = 81$ Fourier samples with $\omega_0 = \frac{2\pi}{2.99T_d}$ rad/s, where T_d denotes the time duration of the sampling kernel and is equal to $20.46\,\mu s$ in our setting. This corresponds to the sampling rate of 1.32 MHz. Prony's annihilating filter technique coupled with Cadzow's denoising method is employed to estimate the time delays $\{t_\ell\}_{\ell=1}^{4}$, followed by amplitude estimation using the least-squares regression. ToF principle is then applied to estimate the spacing between each pair of pins. Figure 3 shows the estimated locations of the pins and the reconstructed signal obtained using the FRI technique. We also plot the locations estimated by the standard matched filtering (MF) technique for the purpose of comparison. As seen in Fig 3, the FRI technique is able to super-resolve thickness of 0.3 mm, which is below the axial resolution limit. On the other hand, MF technique fails to resolve the pair of pins separated by 0.3 mm and estimates only one of the locations of the two pins.

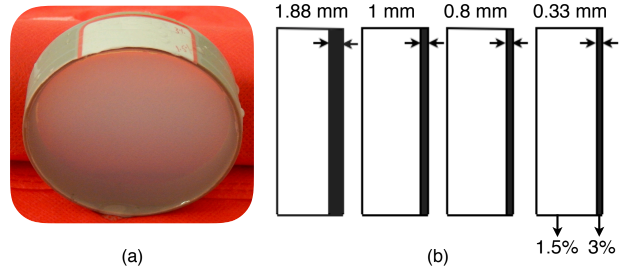

Fig. 5: (a) A double-layered Agarose phantom containing a 19.75 mm thick 1.5% concentration layer and 0.33 mm thick 3% concentration specimen; and (b) a schematic showing double-layered phantoms with varying thickness of the 3% Agarose layer.

IV. Experimental Results

In this section, we study the performance of the FRI technique on the real ultrasound data obtained by imaging specimens which are specifically designed for resolution analysis. For the experiment, we designed double-layered Agarose phantoms (cf. Fig. 5), where the thickness of one of the layers is progressively reduced to a value below the axial resolution limit. The goal is to determine the thickness of the thin layer using the FRI and MF techniques. A schematic and a picture of the experimental setup are shown in Figs. 4(a) and (b), respectively. We prepared a set of four double-layered phantoms having a light layer (1.5% concentration) and a dense layer (3% concentration) (cf. Fig. 5)(a). We consider various thicknesses of the dense layer: 1.88 mm, 1 mm, 0.8 mm, and 0.33 mm as shown in Fig. 5(b).

The Agarose phantoms were probed using an Olympus V323 ultrasound immersion transducer with the center frequency 2.25 MHz. The reflected ultrasound signals were acquired using Tektronix digital storage oscilloscope (DSO) (DPO2014B). A JSR-DPR 300 pulser-receiver was used to trigger the transducer and condition the reflected signal. The -6 dB bandwidth of the transmitted pulse is 2 MHz and the axial resolution limit was computed to be $D = 0.7392$ mm, considering that the velocity of ultrasound in Agarose is 1540 m/s [17].

A total of $|\mathcal{K}| = 89$ Fourier samples were computed with $\omega_0 = 6.17\pi \times 10^4$ radians/sec, which corresponds to the sampling rate of 2.7325 MHz. The FRI reconstruction with

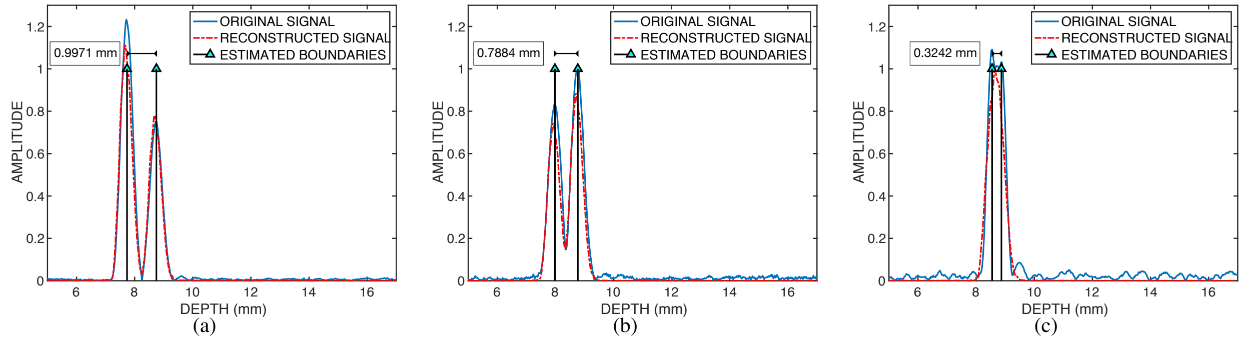

Fig. 6: [Color online] An illustration of FRI reconstruction technique: Envelopes of the original signal and the reconstructed signal along with the estimated boundaries for Agarose phantoms of thicknesses (a) 1 mm, (b) 0.8 mm, and (c) 0.33 mm.

the estimated boundaries are shown in Fig. 6. The signals shown in the figure correspond to the reflections from the 1.5% to 3%, and 3% to water boundaries for three different thicknesses. To demonstrate repeatability of the experiment, we recorded 20 measurements of each phantom. A comparison of the average of the successfully estimated thicknesses ($\left|\frac{\text{Estimated Thickness}-\text{Ground Truth}}{\text{Ground Truth}}\right| < 10\%$) against the ground truth, and the standard deviation of the successful estimates are provided in Table I. For the layer with thickness 0.33 mm, MF technique was not able to resolve the two boundaries. From the experimental results, we infer that the FRI technique is capable of resolving layers with thicknesses up to 0.33 mm, which is about 2.25 times below the conventional limit of $D = 0.7392$ mm, clearly demonstrating super-resolution capability. A comprehensive report on some more experimental results with detailed performance metrics are provided in [16].

TABLE I: Performance comparison of the FRI and MF techniques in terms of the average and standard deviation of the estimated thickness of the Agarose phantoms against the ground-truth.

Sample	**Ground Truth** (mm)	**FRI** **Mean Thickness** (mm)	**FRI** **Standard Deviation** (mm)	**MF** **Mean Thickness** (mm)	**MF** **Standard Deviation** (mm)
1	1.88	1.8758	0.0279	1.8677	0.0295
2	1.00	1.0041	0.0089	1.0176	0.0228
3	0.80	0.7911	0.0358	0.7983	0.0333
4	0.33	0.3193	0.0243	-	-

V. Conclusion

We demonstrated axial super-resolution in 1-D ultrasound imaging by modelling the ultrasound signal as an FRI signal. We showed how such signals can be sampled and reconstructed at sub-Nyquist rates. We demonstrated the applicability of the proposed technique (in comparison with the standard MF technique) on simulated and real ultrasound data acquired by probing Agarose resolution phantoms. The FRI technique outperformed the MF technique in both the cases in terms of resolvability and accuracy in estimating the thicknesses of the layers of the Agarose phantoms. Specifically, the experiments showed that the proposed technique was able to super-resolve Agarose phantoms of thickness which is about 2.25 times below the conventional axial-resolution limit.

References

[1] A. Ng and J. Swanevelder, "Resolution in ultrasound imaging," *Continuing Education in Anaesthesia, Critical Care & Pain*, 2011.
[2] M. Vetterli, P. Marziliano, and T. Blu, "Sampling signals with finite rate of innovation," *IEEE Trans. Signal Process.*, vol. 50, no. 6, pp. 1417–1428, June 2002.
[3] J. Salazar, A. Turó, J. A. Chávez, J. A. Ortega, and M. J. García, "Transducer resolution enhancement by combining different excitation pulses," *Ultrasonics*, vol. 38, no. 1-8, pp. 145–150, 2000.
[4] M. L. Oelze, "Bandwidth and resolution enhancement through pulse compression," *IEEE Trans. Ultrason., Ferroelectr., Freq. Control*, vol. 54, no. 4, pp. 768–781, Apr. 2007.
[5] C. Soussen, J. Idier, E. Carcreff, L. Simon, and C. Potel, "Ultrasonic non destructive testing based on sparse deconvolution," *Journal of Physics: Conference Series*, vol. 353, Mar. 2012.
[6] T. Taxt and G. V. Frolova, "Noise robust one-dimensional blind deconvolution of medical ultrasound images," *IEEE Trans. Ultrason., Ferroelectr., Freq. Control*, vol. 46, no. 2, pp. 291–299, Mar. 1999.
[7] J. A. Jensen, "Real time deconvolution of in-vivo ultrasound images," in *Proc. IEEE Int. Ultrason. Symp. (IUS)*, July 2013, pp. 29–32.
[8] R. Tur, Y. C. Eldar, and Z. Friedman, "Innovation rate sampling of pulse streams with application to ultrasound imaging," *IEEE Trans. Signal Process.*, vol. 59, no. 4, pp. 1827–1842, Apr. 2011.
[9] N. Wagner, Y. C. Eldar, and Z. Friedman, "Compressed beamforming in ultrasound imaging," *IEEE Trans. Signal Process.*, vol. 60, no. 9, pp. 4643–4657, Sept. 2012.
[10] T. Chernyakova and Y. C. Eldar, "Fourier-domain beamforming: The path to compressed ultrasound imaging," *IEEE Trans. Ultrason., Ferroelectr., and Freq. Control*, vol. 61, no. 8, pp. 1252–1267, Aug. 2014.
[11] S. Mulleti, S. Nagesh, R. Langoju, A. Patil, and C. S. Seelamantula, "Ultrasound image reconstruction using the finite-rate-of-innovation principle," in *Proc. IEEE Int. Conf. Image Process. (ICIP)*, 2014, pp. 1728–1732.
[12] P. Stoica and R. L. Moses, *Introduction to Spectral Analysis*. Upper Saddle River, NJ: Prentice Hall, 1997.
[13] J. A. Cadzow, "Signal enhancement – A composite property mapping algorithm," *IEEE Trans. Acoust., Speech, Signal Process.*, vol. 36, no. 1, pp. 49–62, 1988.
[14] J. A. Jensen, "Field: A program for simulating ultrasound systems," in *10th Nordicbaltic Conference on Biomedical Imaging, vol. 4, supplement 1, part 1*, 1996, pp. 351–353.
[15] J. A. Jensen and N. B. Svendsen, "Calculation of pressure fields from arbitrarily shaped, apodized, and excited ultrasound transducers," *IEEE IEEE Trans. Ultrason., Ferroelectr., Freq. Control*, vol. 39, no. 2, pp. 262–267, Mar. 1992.
[16] S. K. Shastri, S. Rudresh, R. Anand, S. Nagesh, C. S. Seelamantula, and A. K. Thittai, "Axial super-resolution in ultrasound imaging with application to non-destructive evaluation," *submitted to Ultrasonics*.
[17] M. M. Burlew, E. L. Madsen, J. A. Zagzebski, R. A. Banjavic, and S. W. Sum, "A new ultrasound tissue-equivalent material." *Radiology*, vol. 134, no. 2, pp. 517–520, 1980.